Superior Valley Polarization and Coherence of 2s Excitons in Monolayer WSe$_2$

Shao-Yu Chen,[1] Thomas Goldstein,[1] Jiayue Tong,[1] Takashi Taniguchi,[2] Kenji Watanabe,[2] and Jun Yan[1,*]

[1]*Department of Physics, University of Massachusetts, Amherst, Massachusetts 01003, USA*
[2]*National Institute of Materials Science, 1-1 Namiki, Tsukuba, Ibaraki 305-0044, Japan*

We report the experimental observation of 2s exciton radiative emission from monolayer tungsten diselenide, enabled by hexagonal boron nitride protected high-quality samples. The 2s luminescence is highly robust and persists up to 150 K, offering a new quantum entity for manipulating the valley degree of freedom. Remarkably, the 2s exciton displays superior valley polarization and coherence than 1s under similar experimental conditions. This observation provides evidence that the Coulomb-exchange-interaction-driven valley-depolarization process, the Maialle-Silva-Sham mechanism, plays an important role in valley excitons of monolayer transition metal dichalcogenides.

The coupled spin-valley physics [1] in monolayer (1L) transition metal dichalcogenide (TMDC) semiconductors has inspired great strides towards realizing valleytronic devices harnessing these two-dimensional (2D) materials [2–5]. The two energetically degenerate 1L TMDC valleys with opposite angular momentum can be selectively populated with circularly polarized optical excitation, and the valley polarization can be detected both optically [2–4] and electrically [5]. Furthermore, a coherent superposition of valley excitons can be generated with linearly polarized light [6] or a sequence of laser pulses with opposite circular polarization [7], which allows for the rotation of the valley pseudospin with a magnetic Zeeman effect or optical Stark effect [8,9]. Such coherent manipulations of the valley pseudospin are at the heart of future quantum valleytronic devices and require a thorough understanding and efficient control of various valley-depolarization and decoherence processes.

In general, intervalley scattering can occur due to both extrinsic mechanisms, such as disorder scattering, and intrinsic mechanisms, such as the Coulomb exchange interaction [10]; the competition between these different valley relaxation channels is a topic under active debate [7,11–13]. So far, many of the valleytronic studies focus on the 1s exciton, the ground state of Coulomb-bound electron-hole pairs, which is readily accessible in 2D TMDC monolayers [2–9,14]. Excitons also have higher energy states that form the hierarchical Rydberg-like series [15–17], similar to hydrogen atoms. It is desirable to access the valley pseudospin of these higher quantum number exciton states, which in previous studies have been employed to demonstrate the exceptionally large exciton binding energy [15–19] and to probe exciton internal quantum transitions [20]. Yet it is relatively challenging to generate radiative emission from these states, as can be understood from Kasha's rule [21]: Photon emission quantum yield is appreciable only for the lowest-energy excited state, which for the charge neutral exciton is the 1s state. In this Letter, we report that, with the efficient removal of disorder and phonon scattering channels, the 2s exciton luminescence from monolayer tungsten diselenide (1L-WSe$_2$) becomes accessible for valleytronic investigations. This is similar to the breaking of Kasha's rule in high-quality GaAs quantum wells [22], where the 2s luminescence becomes observable at low temperatures. We found the 1L-WSe$_2$ 2s exciton luminescence to be robust up to 150 K, providing a new quantum entity for the facile manipulation of valley pseudospins. In contrast to 1s, the 2s exciton exhibits a much higher degree of valley polarization and coherence. This observation could be facilitated in part by the fast population decay of 2s, and our analysis further points to the action of an intervalley Coulomb exchange interaction in TMDC pseudospin propagation, known as the Maialle-Silva-Sham (MSS) mechanism [10], which has been more elusive for charge neutral excitons [11–13] than for trions [6,23,24]. Our studies provide key insights into the TMDC intervalley scattering processes which are essential for developing TMDC-based valleytronic devices.

The 1L-WSe$_2$ samples used in our experiments are mechanically exfoliated from chemical vapor transport grown bulk crystals and are sandwiched between hexagonal boron nitride (hBN) flakes using a dry transfer technique (see Supplemental Material [25]). Figure 1(a) shows the luminescence excited by 2.33 eV photons and the differential reflectance spectra at 20 K. In the upper panel, the luminescence spectrum displays a series of sharp peaks with a narrow linewidth. The peak at 1.724 eV, denoted as X_{1s}^0, is the neutral 1s exciton. Two peaks around 1.69 eV separated by ~7 meV are attributed to the coupled intra- and intervalley trions split by the exchange interaction [6]. In the lower panel, a sharp peak at 1.855 eV with a full width half
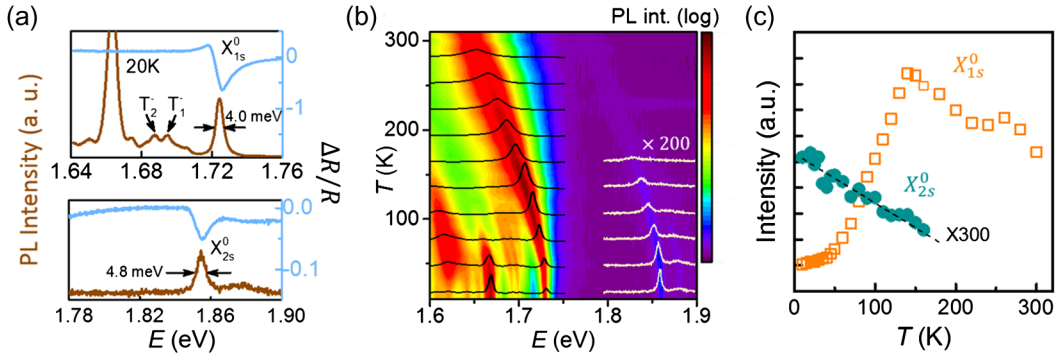
FIG. 1.   (a) The photoluminescence excited by 2.33 eV laser light (brown line) and the differential reflectance (light blue line) spectra at 20 K. The FWHM of $1s$ (X_{1s}^0) and $2s$ (X_{2s}^0) are 4.0 and 4.8 meV, respectively. (b) Photoluminescence spectra plotted as a function of the temperature. Selected spectra at $T = 10$ to 280 K with 30 K steps are displayed. (c) Temperature dependences of $1s$ and $2s$ intensity.

maximum (FWHM) of 4.8 meV appears, and we attribute it to the charge neutral $2s$ exciton luminescence (X_{2s}^0). The differential reflectance exhibits two prominent dips that match well to the X_{1s}^0 and X_{2s}^0 in the luminescence spectra. The near-zero luminescence Stokes shift from the absorption dips [39] and the fully resolved negative trion doublet reflect the good sample quality [6,23,24].

Figure 1(b) shows the temperature dependence of luminescence emission from the sample. Both X_{1s}^0 and X_{2s}^0 blueshift with narrower linewidths at lower temperatures. In Supplemental Material [25], we have performed detailed fittings and found that the peak position and linewidth evolution of X_{1s}^0 and X_{2s}^0 can be described by the same formulations. The temperature-dependent intensities for the two neutral excitons are plotted in Fig. 1(c). The X_{1s}^0 intensity first increases and then decreases, peaking at about 150 K. We note that this is distinct from previous WSe$_2$ samples that display a monotonic $1s$ intensity decrease with a lowering temperature [40], as a result of disorder scattering that depletes bright excitons into thermal equilibrium with lower-energy dark excitons. The excitons in 1L-WSe$_2$ are tightly bound [15] with a large wave function overlap between the constituent electron and hole, giving rise to a large exciton transition dipole oscillator strength and short radiative lifetime [20,41,42]. The nonmonotonic $1s$ intensity temperature dependence is thus a manifestation of out-of-equilibrium exciton radiative recombination becoming more competitive with thermal equilibrium between different quantum channels when disorder in the sample is minimized. In contrast, X_{2s}^0 does not show up until ~150 K, and its intensity keeps increasing with a lowering temperature. Noting that the $2s$-$1s$ exciton energy separation is about 130 meV, in the temperature range of our experiment, the thermal distribution of the $2s$ exciton, unlike $1s$, is largely negligible. The monotonic increase of $2s$ intensity at lower temperatures indicates that the removal of phonon scattering enhances nonequilibrium $2s$ radiative emission and further suggests that the $2s$ exciton also has a fast radiative recombination rate.

We note that there exists some controversy in the assignment of optical features with energies higher than

the $1s$ exciton. Our observed $2s$-$1s$ separation of about 130 meV is consistent with existing differential reflectance [15], photoluminescence excitation (PLE) measurements [43] and up-conversion PL measurements [44], while a separate optical study inferred a much larger $2s$-$1s$ separation of 790 meV [19]. Optical features in hBN-sandwiched WSe$_2$ heterostructures are further complicated by intermaterial exciton-phonon coupling that results in hybrid modes which do not appear in the optical spectra of either hBN or WSe$_2$ alone [45,46]. To confirm that the new emission feature we observe is from the $2s$ exciton, we performed two more control experiments. First, we fabricated an hBN-sandwiched field effect transistor device to tune this new peak by charge doping. We found that both X_{1s}^0 and X_{2s}^0 radiation becomes weaker and eventually disappears when the crystal is doped with electrons or holes
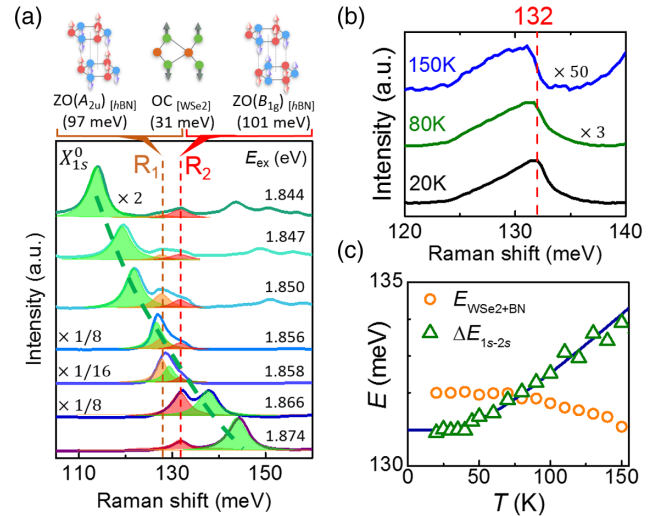

FIG. 2.   (a) Resonant Raman scattering of R_1 and R_2 using photon energies from 1.844 to 1.874 eV. The peaks guided by the green dashed curve are the $1s$ exciton luminescence. (b) Raman scattering of the WSe$_2$/BN combinational modes at 20, 80, and 150 K. The dashed line is aligned with 132 meV. (c) The temperature dependence of $1s$ and $2s$ exciton energy separation ($\Delta E_{1s\text{-}2s}$) and WSe$_2$/BN combinational phonon energy.

(Supplemental Material [25] Fig. S3). This confirms that both X_{1s}^0 and X_{2s}^0 are associated with neutral excitons, consistent with our assignment. Second, we tuned the laser excitation across the X_{2s}^0 energy range to perform one-photon PLE and resonant Raman scattering measurements. The X_{1s}^0 luminescence becomes more intense when the incident photon is in resonance with the X_{2s}^0 energy (Supplemental Material [25] Fig. S4). Furthermore, two Raman bands R_1 and R_2 at 128 and 132 meV become visible in Fig. 2(a), consistent with another recent Raman study that found a broad phonon feature in the range of 128–133 meV (1030–1070 cm^{-1}) [45]. These two bands are assigned as the combinational modes [45,46] arising from the out-of-plane vibrations of WSe$_2$ (OC, out-of-plane chalcogen vibration [47], 31 meV) and hBN (ZO, z-direction optical phonon; the infrared active 97 meV A_{2u} [48] and the optically silent 101 meV B_{1g} [49] phonons). The R_1 and R_2 bands have energies that are quite close to the 1s-2s energy separation; one possibility is that the X_{2s}^0 emission we observe is R_1 and R_2 phonon-exciton replicas of X_{1s}^0. We rule out that interpretation through two observations. One, as can be seen in Fig. 2(a), the combinational phonon bands are composed of two distinct peaks separated by ~4 meV with a nonsymmetric line shape that depends sensitively on the

resonance condition, while the X_{2s}^0 emission spectrum can be well fitted by a Lorentzian function (Fig. 1). Two, we measured the temperature dependence of the combinational phonon bands [Fig. 2(b)] and found that the energy shift is opposite to that of the 1s-2s separation [Fig. 2(c) and Supplemental Material [25] Fig. S5]. This confirms that the X_{2s}^0 emission is not related to R_1 and R_2.

The appearance of the X_{2s}^0 emission in high-quality samples allows us to examine its valleytronic properties. Taking advantage of the valley-dependent optical selection rule [1], we use circularly polarized light to selectively populate one valley and monitor the resultant valley polarization by examining the helicity of optical emission [2–4]. We also use linearly polarized light to create a coherent superposition of excitons in both K and K' valleys; the decoherence of the valley excitons are reflected in the degree of linear polarization of the luminescence emission [6]. Experimentally, we excite our sample at 20 K with σ_+ circularly polarized and H linearly polarized laser light that is detuned by 20 meV above the exciton energy and analyze the collected luminescence emission with σ_+, σ_-, H, and V polarizations; see Fig. 3(a). The valley polarization and coherence are characterized by $P = [(I_{\sigma+\sigma+} - I_{\sigma+\sigma-})/(I_{\sigma+\sigma+} + I_{\sigma+\sigma-})]$ and $C = [(I_{HH} - I_{HV})/(I_{HH} + I_{HV})]$, respectively.
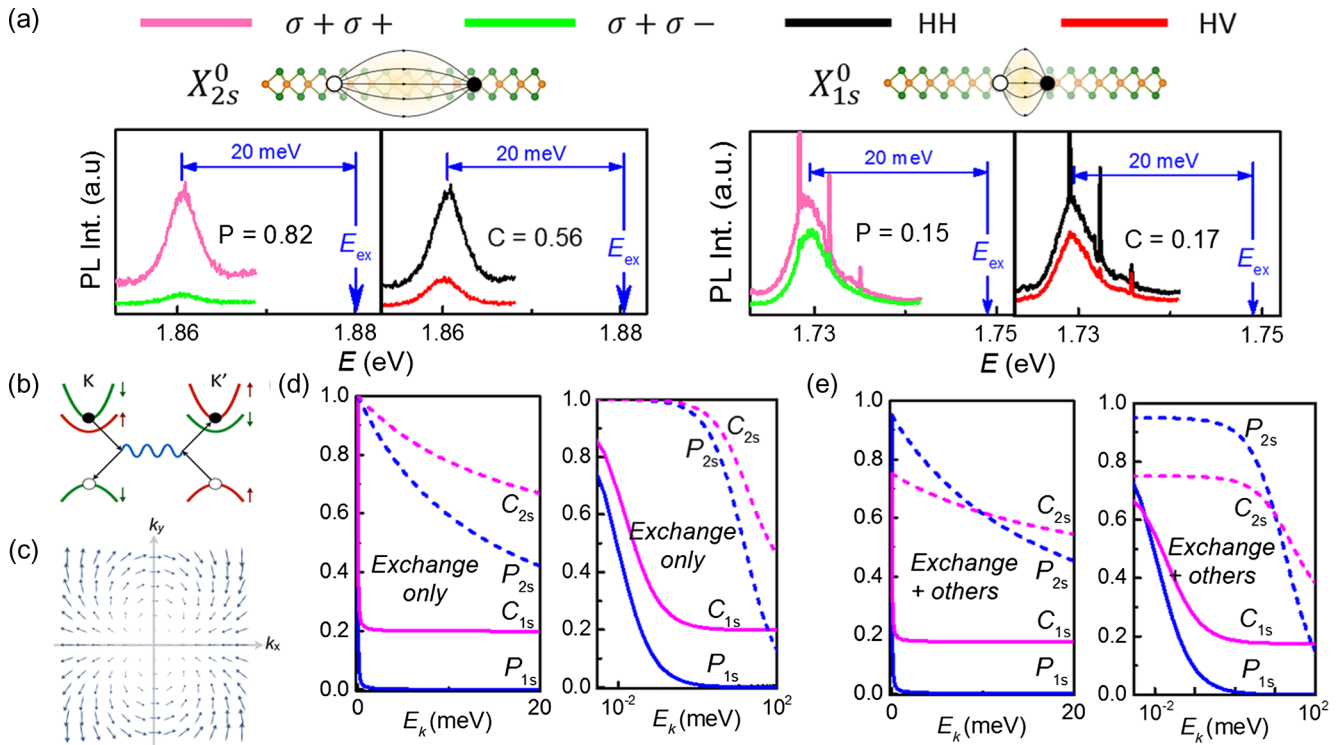

FIG. 3. (a) The circular and linear polarization-resolved photoluminescence of 1L-WSe$_2$ at 20 K with a detuned excitation photon energy at 20 meV above 2s (left) and 1s (right) excitons. (b) A schematic showing the intervalley electron-hole exchange interaction, which induces a pseudospin flip. (c) The strength and direction of the intervalley exchange pseudomagnetic field in k space. (d) The simulated valley coherence (C) and polarization (P) as a function of E_k for 1s and 2s excitons considering pure exchange interactions. The left (right) panel is in the linear (semilog) scale. (e) Simulated C and P considering both exchange interactions and other depolarization and decoherence mechanisms.

From Fig. 3(a), we found the $2s$ excitons to exhibit superior capability in retaining the broken time-reversal symmetry and coherence of incident laser light with $P = 0.82$ and $C = 0.56$. Similar measurements are performed for the $1s$ exciton; see the right panel in Fig. 3(a). Interestingly, its $P = 0.15$ and $C = 0.17$ are significantly smaller than $2s$, although the measurement was performed in the same sample at the same temperature with the laser energy also detuned at 20 meV above the exciton energy.

The superior $2s$ valley polarization could be assisted by its fast population decay rate. As a higher-energy state, the $2s$ exciton possesses decay channels such as the $2s$-$1s$ transition (see Supplemental Material [25]) not available to $1s$. Indeed, X_{2s}^0 has a wider linewidth than X_{1s}^0 [4.8 vs 4.0 meV at 20 K; see Fig. 1(a)]. If we assume that the 0.8 meV linewidth difference is mostly due to a faster population decay and take the $1s$ luminescence emission time to be 2 ps from a recent study [50], we infer a $2s$ lifetime of about 0.6 ps. Noting that the population decay time might be dependent on the sample doping and substrate, we also estimated the ratio of the $1s$ and $2s$ lifetime using another approach: The $2s$ oscillator strength is about 15 times weaker than $1s$ from absorption spectra in Fig. 1, consistent with the value from a recent diamagnetic shift measurement on a similar hBN-sandwiched sample [51], while the low-temperature $1s$ intensity is about 60 times stronger than $2s$ [Fig. 1(c)]. This suggests a decay rate ratio of 4, in reasonable agreement with the above estimation from the linewidth difference. Assuming a phenomenological relation between P, the population and polarization decay time τ and τ_s of $P = [1/(1 + \tau/\tau_s)]$, and using $P = 0.15$ and 0.82 for $1s$ and $2s$, respectively, we find τ_s is about 6 times larger for $2s$ than for $1s$. This indicates that the $2s$ exciton valley polarization is intrinsically more robust than $1s$. Noting that the $2s$ and $1s$ excitons have the same symmetry, intervalley scattering allowed for $1s$ is thus anticipated to also affect the $2s$ valley pseudospins. Quantitatively, however, the scattering rates may differ. In particular, the exchange interaction, capable of inducing intrinsic valley depolarization and decoherence through the MSS mechanism [10], differs substantially for $1s$ and $2s$ excitons. A recent study showed that MSS plays an important role in valley decoherence and observed a coherence time of about 100 fs [7]. Below, we explain the drastically different valley polarization and coherence for $1s$ and $2s$ excitons in the framework of the exchange interaction MSS mechanism.

As illustrated in Fig. 3(b), the strong Coulomb interaction between the photogenerated electrons and holes not only gives rise to an exceptionally large exciton binding energy [15], but also leads to the annihilation of bright excitons in one valley and creation in the other. This exchange of the excitons between the two valleys conserves energy but induces a flipping of the exciton angular momentum and pseudospin, compromising the valley polarization and coherence. For excitons with center-of-mass momentum $\vec{k}$, the intervalley exchange interaction is given by [52]

$$J_{\vec{k}} = -|\psi(r_{eh} = 0)|^2 \frac{a^2 t^2}{E_g^2} V(\vec{k}) k^2 e^{-2i\theta}, \quad (1)$$

where $\psi(r_{eh})$ is the real space wave function for the relative motion between the electron and the hole, $a = 3.32$ Å is the lattice constant of monolayer WSe_2, $t = 1.19$ eV is the hopping energy, $E_g \approx 2$ eV is the band gap, $V(\vec{k})$ is the $\vec{k}$ component of the Coulomb interaction, and θ denotes the direction of $\vec{k}$. Effectively, this exchange interaction introduces a pseudomagnetic field acting on the valley pseudospin of the excitons. The angular dependence in Eq. (1) implies that the direction of the pseudomagnetic field depends on the direction of the exciton wave vector [Fig. 3(c)]. Consider, for example, a set of excitons with the same energy and pseudospin populated on a ring in the $\vec{k}$ space. The pseudomagnetic fields acting on them will have the same magnitude but different directions depending on the direction of $\vec{k}$. This makes the excitons on the ring to precess towards different directions, which, in turn, causes valley depolarization and decoherence as the excitons propagate.

In Eq. (1), $|\psi(r_{eh} = 0)|^2$ describes the probability density for the electron and the hole to spatially overlap. For the $1s$ exciton, this is given approximately by $1/a_B^2$, where $a_B \approx 1.7$ nm [51] is the exciton Bohr radius. In the case of $2s$ excitons, a recent measurement found that the electron-hole separation in $2s$ is about 6.6 nm [51]. Assuming that the $1s$ and $2s$ excitons have about the same mass, the $2s$ exchange interaction is then about 15 times weaker. This difference has an important impact on the exciton valley pseudospin dynamics. In Fig. 3(d), we simulated the pure exchange-interaction-driven valley depolarization and decoherence for excitons with different momentum k and kinetic energy $E_k = k^2/2M$: At $k = 0$, both P and C are equal to 1, since the exchange interaction in Eq. (1) goes to zero at $k = 0$; for nonzero k, both P and C of $1s$ drop steeply at finite E_k, while for $2s$ the decrease is much slower, confirming that $1s$ is more impacted by the exchange depolarization fields.

It is of interest to note that, for both $1s$ and $2s$ simulations in Fig. 3(d), C is always larger than P—this is a hallmark of exciton exchange interaction in 2D [10]: The exchange-interaction-induced pseudomagnetic fields are in the plane of the atomic layer; thus, the out-of-plane pseudospin of valley polarized excitons experiences the pseudomagnetic fields in two directions, while the in-plane pseudospin of the valley coherent excitons is relaxed only by the magnetic field component that is perpendicular to the pseudospin. Experimentally, we have observed C to be larger than P for $1s$ in Fig. 3(a) as well as with many other laser excitations (more data in Supplemental Material [25] Fig. S4), further confirming that the exchange interaction dominates the $1s$ exciton valleytronic behavior. This is consistent with another recent study on high-quality MoS_2 where C is also found to be larger than P [53].

We note that for $2s$ excitons, however, P is significantly larger than C as shown in Fig. 3(a). This suggests that,

with a weaker $2s$ exchange interaction, other decoherence and depolarization mechanisms become more competitive. To account for these additional mechanisms, we have modified the model (see Supplemental Material [25]) such that, even for $k = 0$, P and C are smaller than 1. This relatively simple model captures our observations semiquantitatively: As shown in Fig. 3(e), for excitons with a small kinetic energy ($E_k < 1$ meV), P is mostly larger than C for $2s$ and smaller than C for $1s$, and numerically the $2s$ P and C values are much larger than $1s$.

We finally remark that the exciton can become radiative only if its momentum lies within the light cone, whose boundary corresponds to the $1s$ and $2s$ exciton kinetic energy of ~ 10 μeV. At such small E_k's, the impact of exchange interaction is small. The large difference between P and C for $1s$ and $2s$ agrees with the conjecture that excitons outside the light cone with a larger momentum provide a reservoir where disorder and phonons can scatter them into the light cone, which subsequently radiate [20]. The average exchange interaction that the radiatively recombined excitons experienced is thus much larger than the fields inside the light cone. In Supplemental Material [25], we show that it is possible to reduce the impact of exchange interaction fields on $1s$ by using the small-momentum $2s$ exciton as an alternative reservoir, corroborating another study of WSe$_2$ on SiO$_2$ [54]. Here, with the presence of hBN, the $2s$ exciton can lose the excess ~ 130 meV by emitting zero-momentum hBN-WSe$_2$ combinational phonons [Fig. 2(a)]. This reduces the number of phonons involved from six [54] to two and markedly improves the $1s$ valley coherence and polarization to 0.64 and 0.30, respectively (Supplemental Material [25] Fig. S4).

In conclusion, we have accessed the $2s$ radiative emission in hBN-sandwiched high-quality 1L-WSe$_2$ crystals. The $2s$ luminescence is highly robust and exhibits superior valleytronic properties. Our data provide evidence that the Maialle-Silva-Sham mechanism plays an importance role in the exciton valley decoherence and depolarization, which should be taken into account when developing valleytronic devices.

*Corresponding author.
yan@physics.umass.edu

[1] D. Xiao, G. B. Liu, W. Feng, X. Xu, and W. Yao, Phys. Rev. Lett. 108, 196802 (2012).

[2] K. F. Mak, K. He, J. Shan, and T. F. Heinz, Nat. Nanotechnol. 7, 494 (2012).

[3] H. Zeng, J. Dai, W. Yao, D. Xiao, and X. Cui, Nat. Nanotechnol. 7, 490 (2012).

[4] T. Cao, G. Wang, W. Han, H. Ye, C. Zhu, J. Shi, Q. Niu, P. Tan, E. Wang, B. Liu, and J. Feng, Nat. Commun. 3, 887 (2012).

[5] K. F. Mak, K. L. McGill, J. Park, and P. L. McEuen, Science 344, 1489 (2014).

[6] A. M. Jones, H. Yu, N. J. Ghimire, S. Wu, G. Aivazian, J. S. Ross, B. Zhao, J. Yan, D. G. Mandrus, D. Xiao, W. Yao, and X. Xu, Nat. Nanotechnol. 8, 634 (2013).

[7] K. Hao, G. Moody, F. Wu, C. K. Dass, L. Xu, C.-H. Chen, L. Sun, M.-Y. Li, L.-J. Li, A. H. MacDonald, and X. Li, Nat. Phys. 12, 677 (2016).

[8] R. Schmidt, A. Arora, G. Plechinger, P. Nagler, A. Granados del Águila, M. V. Ballottin, P. C. M. Christianen, S. Michaelis de Vasconcellos, C. Schüller, T. Korn, and R. Bratschitsch, Phys. Rev. Lett. 117, 077402 (2016).

[9] Z. Ye, D. Sun, and T. F. Heinz, Nat. Phys. 13, 26 (2016).

[10] M. Z. Maialle, E. A. de Andrada e Silva, and L. J. Sham, Phys. Rev. B 47, 15776 (1993).

[11] H. Dery and Y. Song, Phys. Rev. B 92, 125431 (2015).

[12] G. Kioseoglou, A. T. Hanbicki, M. Currie, A. L. Friedman, and B. T. Jonker, Sci. Rep. 6, 25041 (2016).

[13] G. Wang, E. Palleau, T. Amand, S. Tongay, X. Marie, and B. Urbaszek, Appl. Phys. Lett. 106, 112101 (2015).

[14] T. Yan, J. Ye, X. Qiao, P. Tan, and X. Zhang, Phys. Chem. Chem. Phys. 19, 3176 (2017).

[15] K. He, N. Kumar, L. Zhao, Z. Wang, K. F. Mak, H. Zhao, and J. Shan, Phys. Rev. Lett. 113, 026803 (2014).

[16] A. Chernikov, T. C. Berkelbach, H. M. Hill, A. Rigosi, Y. Li, O. B. Aslan, D. R. Reichman, M. S. Hybertsen, and T. F. Heinz, Phys. Rev. Lett. 113, 076802 (2014).

[17] H. M. Hill, A. F. Rigosi, C. Roquelet, A. Chernikov, T. C. Berkelbach, D. R. Reichman, M. S. Hybertsen, L. E. Brus, and T. F. Heinz, Nano Lett. 15, 2992 (2015).

[18] Z. Ye, T. Cao, K. O'Brien, H. Zhu, X. Yin, Y. Wang, S. G. Louie, and X. Zhang, Nature (London) 513, 214 (2014).

[19] A. T. Hanbicki, M. Currie, G. Kioseoglou, A. L. Friedman, and B. T. Jonker, Solid State Commun. 203, 16 (2015).

[20] C. Poellmann, P. Steinleitner, U. Leierseder, P. Nagler, G. Plechinger, M. Porer, R. Bratschitsch, C. Schüller, T. Korn, and R. Huber, Nat. Mater. 14, 889 (2015).

[21] M. Kasha, Discuss. Faraday Soc. 9, 14 (1950).

[22] K. J. Moore, P. Dawson, and C. T. Foxon, Phys. Rev. B 34, 6022 (1986).

[23] A. M. Jones, H. Yu, J. R. Schaibley, J. Yan, D. G. Mandrus, T. Taniguchi, K. Watanabe, H. Dery, W. Yao, and X. Xu, Nat. Phys. 12, 323 (2015).

[24] A. Singh, K. Tran, M. Kolarczik, J. Seifert, Y. Wang, K. Hao, D. Pleskot, N. M. Gabor, S. Helmrich, N. Owschimikow, U. Woggon, and X. Li, Phys. Rev. Lett. 117, 257402 (2016).

[25] See Supplemental Material at http://link.aps.org/supplemental/10.1103/PhysRevLett.120.046402, which includes Supplemental Refs. [26–38], for additional details on the sample preparation, optical setup, supporting experiments, and analysis, as well as valley-depolarization and decoherence model.

[26] L. Wang, I. Meric, P. Y. Huang, Q. Gao, Y. Gao, H. Tran, T. Taniguchi, K. Watanabe, L. M. Campos, D. A. Muller,

J. Guo, P. Kim, J. Hone, K. L. Shepard, and C. R. Dean, Science **342**, 614 (2013).

[27] S.-Y. Chen, T. Goldstein, D. Venkataraman, A. Ramasubramaniam, and J. Yan, Nano Lett. **16**, 5852 (2016).

[28] S.-Y. Chen, C. H. Naylor, T. Goldstein, A. T. C. Johnson, and J. Yan, ACS Nano **11**, 814 (2017).

[29] T. Goldstein, S.-Y. Chen, J. Tong, D. Xiao, A. Ramasubramaniam, and J. Yan, Sci. Rep. **6**, 28024 (2016).

[30] K. P. O'Donnell and X. Chen, Appl. Phys. Lett. **58**, 2924 (1991).

[31] M. Selig, G. Berghäuser, A. Raja, P. Nagler, C. Schüller, T. F. Heinz, T. Korn, A. Chernikov, E. Malic, and A. Knorr, Nat. Commun. **7**, 13279 (2016).

[32] H. Sahin, S. Tongay, S. Horzum, W. Fan, J. Zhou, J. Li, J. Wu, and F. M. Peeters, Phys. Rev. B **87**, 165409 (2013).

[33] G. Moody, C. Kavir Dass, K. Hao, C.-H. Chen, L.-J. Li, A. Singh, K. Tran, G. Clark, X. Xu, G. Berghäuser, E. Malic, A. Knorr, and X. Li, Nat. Commun. **6**, 8315 (2015).

[34] B. Fallahazad, H. C. P. Movva, K. Kim, S. Larentis, T. Taniguchi, K. Watanabe, S. K. Banerjee, and E. Tutuc, Phys. Rev. Lett. **116**, 086601 (2016).

[35] G.-B. Liu, W.-Y. Shan, Y. Yao, W. Yao, and D. Xiao, Phys. Rev. B **88**, 085433 (2013).

[36] S. Fang, R. Kuate Defo, S. N. Shirodkar, S. Lieu, G. A. Tritsaris, and E. Kaxiras, Phys. Rev. B **92**, 205108 (2015).

[37] T. C. Berkelbach, M. S. Hybertsen, and D. R. Reichman, Phys. Rev. B **88**, 045318 (2013).

[38] D. Y. Qiu, F. H. da Jornada, and S. G. Louie, Phys. Rev. Lett. **111**, 216805 (2013).

[39] F. Yang, M. Wilkinson, E. J. Austin, and K. P. O'Donnell, Phys. Rev. Lett. **70**, 323 (1993).

[40] X.-X. Zhang, Y. You, S. Y. F. Zhao, and T. F. Heinz, Phys. Rev. Lett. **115**, 257403 (2015).

[41] M. Palummo, M. Bernardi, and J. C. Grossman, Nano Lett. **15**, 2794 (2015).

[42] H. Wang, C. Zhang, W. Chan, C. Manolatou, S. Tiwari, and F. Rana, Phys. Rev. B **93**, 045407 (2016).

[43] G. Wang, X. Marie, I. Gerber, T. Amand, D. Lagarde, L. Bouet, M. Vidal, A. Balocchi, and B. Urbaszek, Phys. Rev. Lett. **114**, 097403 (2015).

[44] M. Manca, M. M. Glazov, C. Robert, F. Cadiz, T. Taniguchi, K. Watanabe, E. Courtade, T. Amand, P. Renucci, X. Marie, G. Wang, and B. Urbaszek, Nat. Commun. **8**, 14927 (2017).

[45] C. Jin, J. Kim, J. Suh, Z. Shi, B. Chen, X. Fan, M. Kam, K. Watanabe, T. Taniguchi, S. Tongay, A. Zettl, J. Wu, and F. Wang, Nat. Phys. **13**, 127 (2017).

[46] C. M. Chow, H. Yu, A. M. Jones, J. Yan, D. G. Mandrus, T. Taniguchi, K. Watanabe, W. Yao, and X. Xu, Nano Lett. **17**, 1194 (2017).

[47] S.-Y. Chen, C. Zheng, M. S. Fuhrer, and J. Yan, Nano Lett. **15**, 2526 (2015).

[48] R. Geick, C. H. Perry, and G. Rupprecht, Phys. Rev. **146**, 543 (1966).

[49] J. Serrano, A. Bosak, R. Arenal, M. Krisch, K. Watanabe, T. Taniguchi, H. Kanda, A. Rubio, and L. Wirtz, Phys. Rev. Lett. **98**, 095503 (2007).

[50] C. Robert, D. Lagarde, F. Cadiz, G. Wang, B. Lassagne, T. Amand, A. Balocchi, P. Renucci, S. Tongay, B. Urbaszek, and X. Marie, Phys. Rev. B **93**, 205423 (2016).

[51] A. V. Stier, N. P. Wilson, K. A. Velizhanin, J. Kono, X. Xu, and S. A. Crooker, arXiv:1709.00123 [Phys Rev. Lett. (to be published)].

[52] H. Yu, G.-B. Liu, P. Gong, X. Xu, and W. Yao, Nat. Commun. **5**, 3876 (2014).

[53] F. Cadiz, E. Courtade, C. Robert, G. Wang, Y. Shen, H. Cai, T. Taniguchi, K. Watanabe, H. Carrere, D. Lagarde, M. Manca, T. Amand, P. Renucci, S. Tongay, X. Marie, and B. Urbaszek, Phys. Rev. X **7**, 021026 (2017).

[54] G. Wang, M. M. Glazov, C. Robert, T. Amand, X. Marie, and B. Urbaszek, Phys. Rev. Lett. **115**, 117401 (2015).